lization of the vias. Using a flash of gold on the aluminium ground plane provided the low resistance contact to the test housing. The use of silicon micromachining has enabled these devices to be produced on a small scale. Integration with other devices on silicon can now be realized; further development in further reducing the size with bulk micromachining the silicon dielectric has also been proposed.

ACKNOWLEDGMENT

The authors thank Colin Bird and his industrial sponsor Selex Airborne systems. They also thank Robert Greed at BAE Systems ATC for continued help and BAE ATC at Filton in Bristol for the fabrication of the filters.

REFERENCES

1. G.L. Matthaei, Interdigital band-pass filters, Proc IRE, New York, NY (1962), 479–491.
2. J.S. Hong and M.J. Lancaster, Microstrip filters for RF/microwave applications, Wiley, New York, NY 2001.
3. K. Ma and J. Ma, A miniaturized silicon-based ground ring guarded patch resonator and filter, IEEE Microwave Wireless Compon Lett 15 (2005), 478–480.
4. D.S. Yu and C.F. Cheng, Narrow-band band-pass filters on silicon substrates at 30 GHz, IEEE MTT-S, Fort Worth, TX (2004), 1467–1470.
5. M.J. Madou, Fundamentals of microfabrication, Section Edition, CRC Press, Chapter 4.
6. H.-K. Pang, K.-M. Ho, K.-W. Tam, and R.P. Martins, A compact microstrip λ/4-SIR interdigital bandpass filter with extended stopband, IEEE MTT-S Dig, Fort Worth, TX (2004), 1621–1625.

SUBSTRUCTURING APPROACH TO OPTIMIZATION OF MATCHING FOR PHOTONIC CRYSTAL WAVEGUIDES

Ben Z. Steinberg, Amir Boag, and Orli Hershkoviz
School of Electrical Engineering
Tel Aviv University
Tel Aviv 69978, Israel

Received 2 March 2006

ABSTRACT: *A substructuring approach for numerical optimization of photonic crystal devices is proposed and demonstrated. Specifically, we consider the matching of coupled cavity waveguides (CCW's)—known also as coupled resonators optical waveguides (CROWs)—to free space. In this approach, one separates a priori between the invariant main structure that consists most of the PhC and the CCW, and the substructure that consists of a small portion of the CCW and evolves along the optimization course. Specific examples of matching configurations with insertion loss as low as few percent are presented.* © 2006 Wiley Periodicals, Inc. Microwave Opt Technol Lett 48: 1866–1871, 2006; Published online in Wiley InterScience (www.interscience.wiley.com). DOI 10.1002/mop.21766

Key words: *photonic crystals; guided waves; coupled cavity waveguide; coupled resonator optical waveguide-CROW; resonators*

1. INTRODUCTION

Photonic crystals (PhC) have a great potential for applications in optical devices [1]. Owing to their relatively high manufacturing costs, it is vital to have precise design tools that can simulate device configurations, predict their performance for a wide range of parameters, and obtain the optimal parameters that yield best performance. The purpose of this work is to develop an approach to optimize the matching of PhC waveguides to external structures, and to apply this approach to match a PhC-based coupled-cavity waveguide (CCW) [2, 3] to free space. Preliminary results have been reported in Ref. 4 and 5. Generally, in its PhC realization, the CCW comprises a linear array of widely-separated, equally-spaced, and identical microcavities in a photonic crystal. Each microcavity is manifested by a local defect that can localize light at a frequency within the original photonic band gap [1, 3]. A 2D example of a PhC comprising dielectric cylinders in a homogeneous background is shown in Figure 1. In this example, the microcavities are created by removing the corresponding dielectric cylinders. The waveguiding mechanism is based on tunneling of light between adjacent microcavities. The CCW constitutes a narrow-band low group velocity guiding structure, as opposed to a more common photonic crystal waveguide obtained by creating a contiguous line of defects, which supports a relatively wide-band guiding of optical signals [1]. The CCW central frequency is determined by the nature of its basic building block—the local defect, while the CCW bandwidth and group velocity are determined by the intercavity spacing [2, 3]. Because of these properties, this device is potentially an ideal candidate for optical communication tasks such as optical filtering and routing, optical delay lines [6], and optical parametric amplifiers [7]. Furthermore, it has recently been shown that the CCW can also be used to design ultra-compact optical gyroscopes [8].

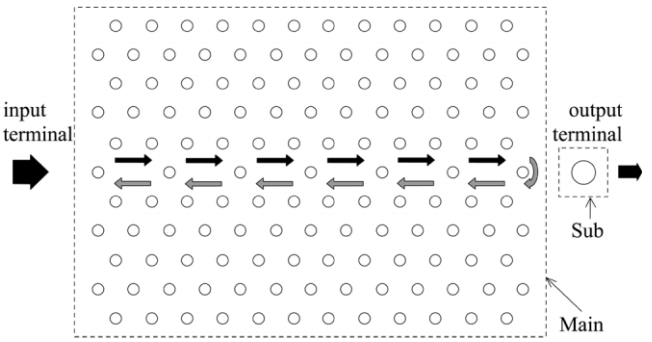

Figure 1 Transmission in photonic crystal coupled cavity waveguide

Clearly, the ability to match the CCW to the medium or structure surrounding the photonic crystal plays a pivotal role in using this device for the applications discussed above. The design of a matching structure can be formulated as an optimization problem: find the geometry of the output port that minimizes the back-reflections at the CCW terminal—see Figure 1. In recent years attention has been devoted to the problem of optimization of various aspects of photonic crystal devices [9–11]. Especial effort was also devoted to the problem of transmission through sharp bends [12–14]. Topology optimization [15] together with the moving asymptotes method [16] was used for optimization of bends [17, 18], T-junction [19], and termination of PhC waveguide [20]. A typical method for photonic crystal optimization comprises adding or removing cylinders or holes inside the photonic crystal and changing their radii or locations. This method was successfully applied for optimization of bends [14, 21, 22] and Y-junction [9]. Other works validated this technique in terms of transmission line theory [23] and used it for matching a finite length photonic crystal waveguide. Stochastic optimization methods based on the geometric modifications were also adapted for photonic crystal optimization. T-junction [11] was optimized using a genetic algorithm. Simulated annealing was used for bend optimization [10]. How-

ever, these works were concerned with the conventional photonic crystal waveguides, and did not address matching of CCWs. Also, in terms of numerical efficacy, they did not take advantage of the fact that only an extremely limited region of the crystal geometry has to be modified during the optimization search.

Our goal is to develop an optimization procedure that can address efficiently the CCW matching problem. Few important points should be taken into consideration. First, the reflection at the CCW terminal (see Fig. 1) depends strongly on the CCW properties including the surrounding PhC structure. Therefore, to determine the reflection loss in a sufficiently precise manner, the entire propagation/scattering problem associated with the CCW and its output port has to be solved. The typical solution thus involves the scattering from few hundreds of photonic crystal cells, for which no perfect periodicity can be assumed. The computational complexity typically scales as a high power of the number of unknowns, thus making each solution numerically expensive. Second, any optimization process requires the computation of the solution for many scattering problems differing by the geometry at the CCW exit port. We therefore find that the total numerical cost of such a repetitive solution is too high to be practically implemented on standard computing platforms.

A potential remedy to the difficulties described above is offered by the fact that a large portion of the dielectric structure—consisting of the PhC and the CCW—stays unchanged during the optimization course. We term this portion of the geometry as the main structure. It is only a small region near the output port that undergoes geometrical variations in seeking the optimum. We term this portion of the structure as the substructure (see Fig. 1). This observation naturally calls for a substructuring approach. To that end, the impedance matrix representing the entire scattering problem is partitioned into four blocks representing the main structure, the substructure, and the main-to-sub and sub-to-main scattering operators. Then, using the Schur's complement approach, a new reduced formulation can be written, whose size is effectively that of the substructure and in which the effect of the main structure is expressed via an operator that need not be repeatedly inverted at each optimization cycle. Thus, we show that for a structure consisting of typically 200 PhC cells, a reduction of the computation complexity by a factor of nearly two orders of magnitude is obtained. This substructuring methodology enables one to perform matching optimizations for large and complex structures at a reasonable numerical cost. In the example considered here, our optimization procedure yields a very simple matching structure consisting of only a single matching cylinder and attained transmission of more than 97% with good output beam collimation.

2. PROBLEM DESCRIPTION AND FORMULATION

The general approach developed here applies to two-dimensional (2D) and three-dimensional (3D) photonic crystal structures. We consider the problem of a CCW comprising N_{cav} microcavities embedded in a finite size photonic crystal structure. An incident wave hits from the left the photonic crystal within which our CCW is placed—see example in Figure 1. A guided wave is thus excited within the CCW and propagates rightward toward the output terminal, where the aforementioned reflection and transmission take place. According to the well-established theory [3], the right- and left-propagating electromagnetic fields along the CCW are described by $E^+ e^{-j\beta n}$ and $E^- e^{-j\beta n}$, respectively, where n designates the cavity number. The reflection coefficient is defined as $\Gamma = E^-/E^+$. The standing wave created by the left- and right-propagating waves can be used to measure the mismatch at the output terminal. Thus, we define the standing wave ratio SWR as the ratio between the maximal and minimal absolute values of the electric field modes evaluated at each of the CCW cavities,

$$\text{SWR} = \text{medmax}_m\{|E(c_0 + m\mathbf{b}|\}\min_n\{|E(c_0 + m\mathbf{b}|\} \quad m, n = 0,\cdots,N_{\text{cav}}-1, \quad (1)$$

where E is the electric field, c_0 is a reference point chosen within the first cavity, where the intensity of the cavity excitation can be conveniently measured (for symmetric cavity modes it is the cavity center), and $\mathbf{b}$ is the intercavity spacing vector. In the general case $\mathbf{b} = \sum_{i=1}^{d} m_i \mathbf{a}_i$, where $\mathbf{a}_i$ is the fundamental lattice vector of the photonic crystal, m_i is the integer, and d is the photonic crystal dimension. Clearly, SWR $\geq$ 1, and a perfect matching with no insertion loss (no reflection at the right end) corresponds to SWR = 1. Note that for a finite number of cavities the relation $\text{SWR} = (1+|\Gamma|)/(1-|\Gamma|)$ is only an approximate one and becomes increasingly accurate as $N_{\text{cav}} \to \infty$. Our purpose is to minimize the SWR by modifying the waveguide structure in the neighborhood of the right-end terminal, thus minimizing reflection from this end of the waveguide and maximizing transmission.

3. MATCHING OPTIMIZATION AND SUBSTRUCTURING

In general, the electromagnetic fields in the structure can be described as an exact solution of an integral equation formulation. Using a standard numerical technique such as the multi-filaments method [3, 24], the continuous formulation is cast in the form of a matrix equation formulation,

$$[Z][I] = [V], \quad (2)$$

where the $N \times N$ matrix $[Z]$ represents the mutual interactions between induced sources and fields inside the photonic crystal, the known N-vector $[V]$ describes the excitation of the system, and the N-vector $[I]$ comprises the N unknowns representing the induced currents excited within the structure as a response to the excitation. Once the system is solved and $[I]$ is known, the actual electromagnetic fields are readily obtained from $[I]$ by direct summation, and the SWR in Eq. (1) can be computed.

Because of the resonant nature of the problem expressed by a high condition number of matrix $[Z]$, noniterative solution of Eq. (2) is preferred. On the other hand, computational complexity of direct solvers scales as N^3 and becomes quite high for the relatively large problems of interest here. This difficulty is further exacerbated, since any optimization process involves a large number of "forward" solutions of Eq. (2). Therefore, optimization of realistic configurations becomes prohibitive if no special effort is taken to reduce the computational cost of a single forward solution and hence the corresponding computational cost of the entire optimization process. Towards this end, we take advantage of the fact that in our problem the "best geometry" search is of a local nature; only a very limited region of the crystal structure is modified by the optimization process, while the rest of the structure remains completely unchanged during the optimization process. Referring to their different roles and sizes, we term the modified and unmodified regions as the *sub* and *main* structures, respectively. This partition is shown schematically in Figure 1. For any realistic configuration, the substructure is by far smaller than the main structure. Thus, we assume that our device is represented by $N_m + N_s = N$ unknowns, while N_m unknowns are associated with the invariant-main structure, and N_s unknowns belong to the substructure undergoing changes. We have $N_m >> N_s$. Let us define the term *computing cycle* as the full process of finding the

solution for a given geometry or a given set of parameters. Then the computational complexity of the straightforward approach for optimization process with N^c computing cycles is of $O(N^c(N_m + N_s)^3) \approx O(N^c N_m^3)$ operations.

Toward reducing the complexity of the optimization process, we propose a substructuring methodology, where the matrix Eq. (2) is partitioned into submatrices, representing the self and mutual interactions of the aforementioned photonic crystal main and substructures. By a straightforward rearrangement of the rows and columns of $[Z]$ and, accordingly, of the entries of $[I]$ and $[V]$, we get a partitioned matrix equation

$$\begin{bmatrix} [Z_{mm}] & [Z_{ms}] \\ [Z_{sm}] & [Z_{ss}] \end{bmatrix} \begin{bmatrix} [I_m] \\ [I_s] \end{bmatrix} = \begin{bmatrix} [V_m] \\ [V_s] \end{bmatrix}. \quad (3)$$

Formally solving the upper half of (3) for the main structure currents $[I_m]$ and substituting it in the lower half, we obtain an equation written solely for the substructure unknowns $[I_s]$

$$([Z_{ss}] - [Z_{sm}][Z_{nm}]^{-1}[Z_{ms}])[I_s] = [V_s] - [Z_{sm}][Z_{mm}]^{-1}[V_m], \quad (4)$$

which has much smaller dimensions ($N_s << N_m$). We can simplify this equation further by defining a new matrix $[Z_0] = [Z_{mm}]^{-1}$ and a new vector $[V_0] = [Z_0][V_m]$. These matrix and vector are computed only once and therefore can be used for different settings of the substructure. In (4), we reduced (3) of size $(N_m + N_s) \times (N_m + N_s)$ to a matrix equation with dimension $N_s \times N_s$ and hence its solution can be found much faster. Because of the large ratio between N_m and N_s, the major computational cost in solving Eq. (4) stems not from the $N_s \times N_s$-matrix inversion, but from the matrix multiplications $[Z_{sm}][Z_{mm}]^{-1}[Z_{ms}]$. Thus, the computational complexity (operation counts) of the entire optimization process based on our substructuring approach is estimated as

$$O(N_m^3) + O(N^c N_m^2 N_s). \quad (5)$$

The first term in (5) is due to the large matrix ($N_m \times N_m$) single inversion ($[Z_{mm}]^{-1}$), and the second term is due to the fact that the matrix multiplication has to be performed at each computing cycle since the small matrices $[Z_{sm}]$, $[Z_{ms}]$ are changed from one computing cycle to the next.

Figure 2 compares the computational complexity (operation-counts) associated with the substructuring approach, to that of the conventional approach, for a problem consisting of a main structure with 173 dielectric cylinders and a substructure of a single dielectric cylinder (see Fig. 1), and the numerical example in Section 3, where each cylinder corresponds to 24 unknowns. At the first cycle the two approaches are of the same order of complexity due to the costly (single) inversion or factorization of $[Z_{mm}]$ that cannot be avoided. However, as the number of cycles increases, the substructuring approach becomes increasingly advantageous. In our examples, the number of computation cycles, N^c, exceeds 50, thus substructuring reduces complexity by nearly two orders of magnitude.

4. NUMERICAL EXAMPLES

In this section we present results of matching optimization using the substructuring methodology. For simplicity, the technique is tested with 2D PhC comprising dielectric cylinders. In our models, the cylinder's axis is parallel to the z-axis of Cartesian coordinate system. We assume that the material permeability is always μ_0.

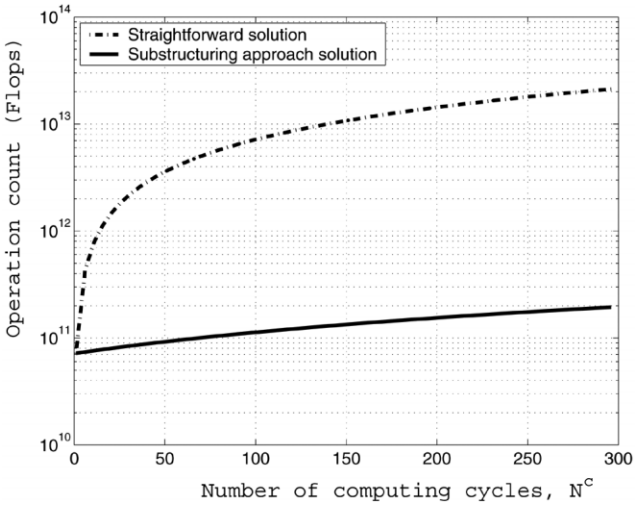

Figure 2 Comparison of the computational complexities

The multi-filaments method [3, 24] is used to construct the basic method of moment matrix equation given in (2).

The specific photonic crystal-based CCW used in our simulation is shown in Figure 1. It comprises 173 dielectric cylinders. The crystal geometrical parameters are as follows (in arbitrary units): cylinder radius, 0.6 length units; cylinder separation, 4 length units. The relative permittivity of the cylinders dielectric material is $\varepsilon_r = 8.41$, and the relative permittivity of the background is 1. A basic microcavity is formed by removing a single cylinder as shown in Figure 1. This microcavity possesses a resonant wavelength $\lambda_0 = 9.06$ [3]. A CCW is now created by a linear array of eight microcavities, with an intercavity spacing of two hexagonal unit cells along the x-axis. With these parameters, the resulting CCW guides optical signal with wavelengths in the range of $8.8 \leq \lambda \leq 9.3$ length units (so that its transmission bandwidth is ~0.5 length units, centered around the isolated microcavity resonance $\lambda_0 = 9.06$) (see Ref. 3 for details). Figure 3 shows this CCW excited by an incident TM plane-wave propagating from left to right. However, in addition to the forward wave, the backward propagating wave is excited due to reflection at the CCW output terminal. The pronounced uneven excitation of the cavities comprising the CCW in Figure 3, leading clearly to

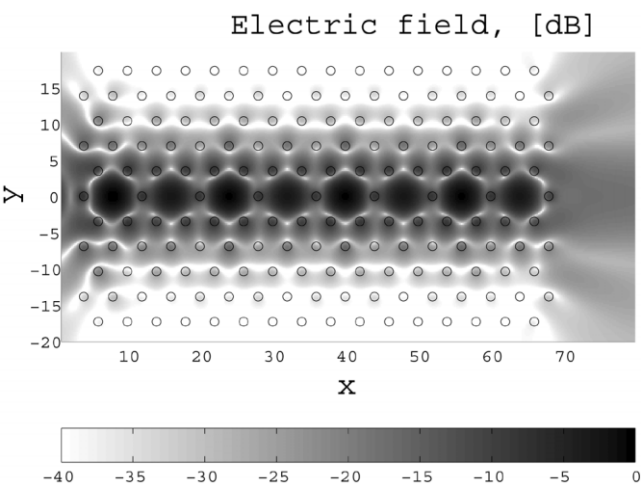

Figure 3 Electric field in the coupled cavity waveguide before optimization

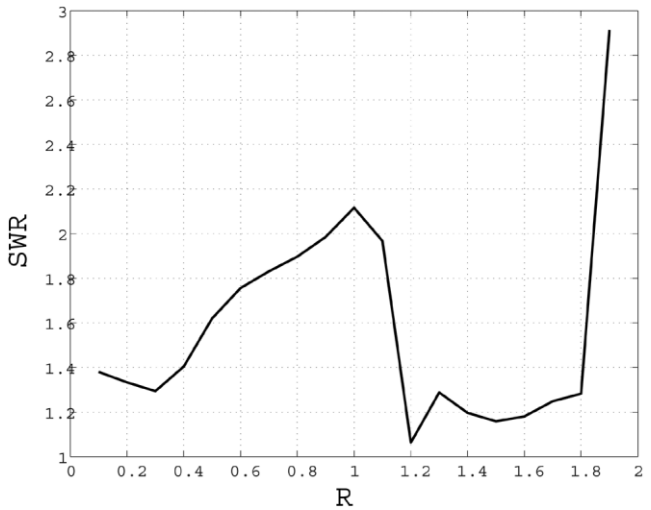

Figure 4 SWR in CCW versus the matching post radius

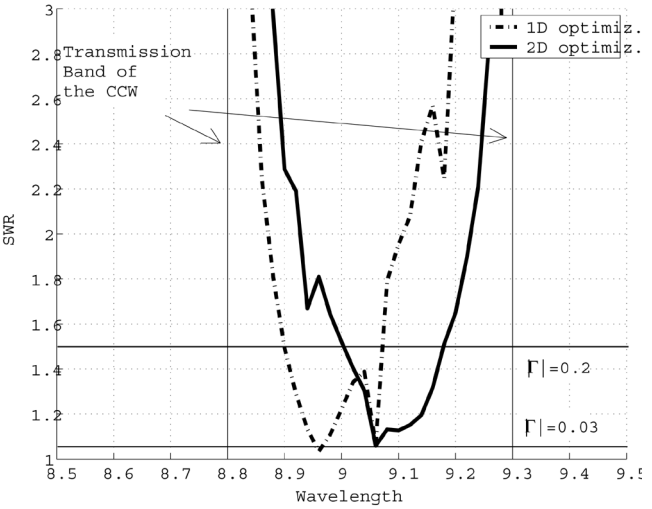

Figure 6 SWR of the optimized waveguides versus wavelength

SWR $>$ 1, is nothing but a result of the interference between the forward and backward propagating waves.

To match this CCW to the external domain, a single cylinder—the matching post—placed in the external space to the right of the main structure is chosen as a substructure (see Fig. 1). Optimization is performed over the matching post radius and *x*-coordinate. Different strategies of the optimization search in the 2D space of radius and location can be applied here. We have tested two of them: a series of alternating one-dimensional (1D) optimizations and a full 2D search optimization. In both, we apply the substructuring approach.

The first goal of the alternating 1D optimizations approach is to find the radius of the substructure that minimizes the value of SWR, for a matching post located on the *x*-axis at the distance of 4 length units from the last *x*-placed waveguide cylinder. The dependence of the SWR on radius of the substructure's post is shown in Figure 4. In the next step, we scan over locations of the substructure's post, using the radius obtained in the previous step. The results are shown in Figure 5. One can see that for the same radius there are a few minima. At the first one, SWR is equal to 1.063. This corresponds to the amplitude reflection coefficient of about 3.05%. Two important factors should be examined to assess the quality of this matching geometry: the matching bandwidth and the beam collimation at the region of the output terminal. Figure 6 shows the SWR as a function of wavelength. It is seen that SWR $\leq$ 1.5 ($\Gamma \leq 0.2$) for almost 30% of the CCW transmission bandwidth. The electric field distribution inside and outside of the structure and at the central matching wavelength ($\lambda = \lambda_0 = 9.06$) is shown in Figure 7. It is evident from the figure that while the CCW microcavities are evenly excited (leading to SWR $\approx$ 1), the beam collimation quality at the output terminal domain is quite poor. Indeed, Figure 8 shows the field distribution before and after the matching normalized relative to the incident field at a distance of one wavelength away from the output terminal into the external medium. Before the matching, the output terminal forms a relatively well-collimated beam, with a peak intensity of about 7.2 dB relative to the incident field. It is seen that the beam collimation has been completely degraded by the matching post. Thus, although the matching to free space is very good at this wavelength and most of the energy is indeed transmitted to the external medium, the beam peak intensity is considerably lower than that of the nonoptimized case (see Fig. 8), as a large portion of it has been scattered into the beam side lobes.

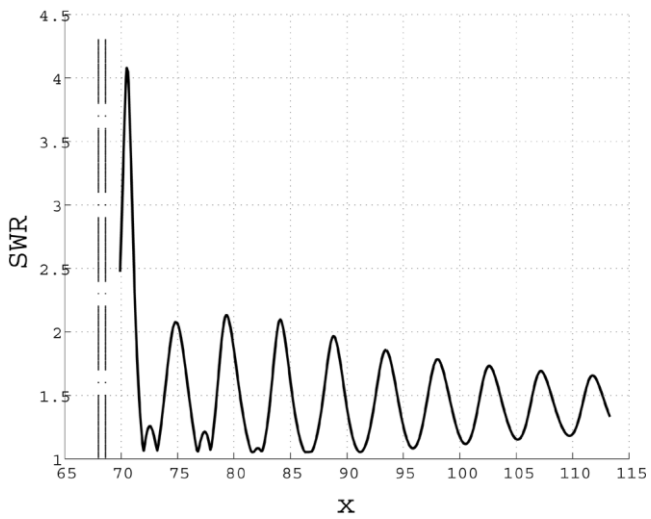

Figure 5 SWR versus the matching post displacement along the *x*-axis. The two lines on the left side show the center and the right side of the last post in the main structure

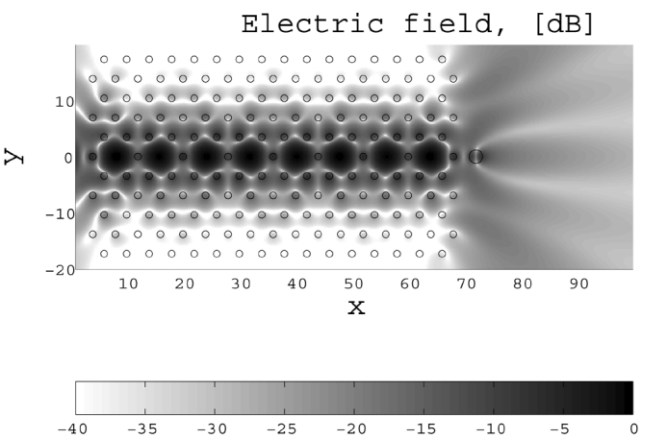

Figure 7 The electric field of the matched CCW after a series of 1D optimizations

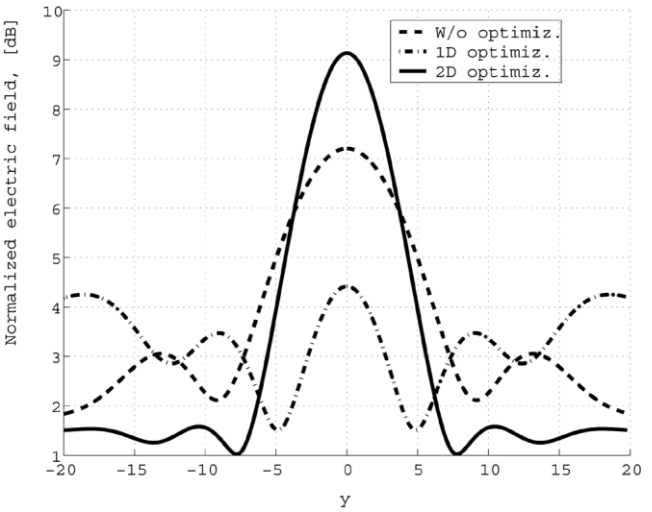

Figure 8 Comparison of the amplitude of the electric fields along the *y*-axis at a distance of one wavelength (9.06 length units) away from the output terminal: before optimization, after a series of the 1D optimizations, and after the 2D optimization

Clearly, these design parameters can be further tuned by additional alternating iterations. However, here we shall not pursue this approach further. Rather, we turn to suggest a 2D search route, where optimization is performed simultaneously along the radius and distance axes. At each computing cycle, the SWR is checked at 16 points located on a rectangular domain surrounding the current optimum R_0,d_0. The point with minimal value of SWR is chosen as the next optimum, and the process is repeated. This search trace is shown in Figure 9. The optimal solution gives SWR of 1.059, which corresponds to the reflection coefficient of about 2.87%. Such approach solves the main disadvantage of the 1D optimizations: the output beam is well collimated as shown in Figures 10 and 8. Figure 6 shows the SWR as a function of wavelength, as obtained for this optimal point. It is seen that the matching bandwidth here is essentially the same as that of the previous case.

5. CONCLUSIONS

We proposed a novel substructuring approach to matching optimization for photonic crystal waveguides. As an example, the proposed algorithm is employed to design a geometry consisting of a CCW and a single matching cylinder. At the optimal points, the reflection coefficients are smaller than 0.03 at the design frequency within the transmission band while maintaining good output beam collimation, and is generally smaller than 0.2 for about one third of the CCW bandwidth.

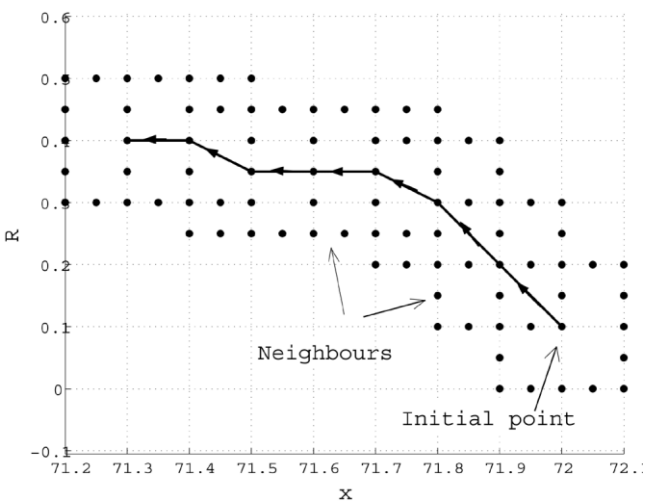

Figure 9 2D optimization process

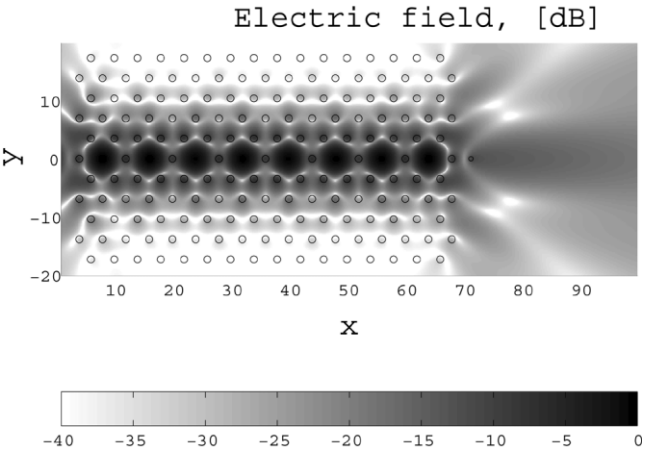

Figure 10 The electric field of the matched CCW after the 2D optimization

REFERENCES

1. J.D. Joannopoulos, R.D. Meade, and J.N. Winn, Photonic crystals: Molding the flow of light, Princeton University Press, Princeton, NJ, 1995.
2. A. Yariv, Y. Xu, R.K. Lee, and A. Scherer, Coupled-resonator optical waveguide: A proposal and analysis, Opt Lett 24 (1999), 711–713.
3. A. Boag and B.Z. Steinberg, Narrow-band microcavity waveguides in photonic crystals, J Opt Soc Am A 18 (2001), 2799–2805.
4. A. Boag, B.Z. Steinberg, and O. Bushmakin, Matching of narrow-band photonic crystal filters and waveguides to free space and dielectric waveguides, In: URSI Radio Science Meeting, 2003.
5. O. Hershkoviz, B.Z. Steinberg, and A. Boag, Substructuring approach to optimization of matching structures for photonic crystal waveguides, In: 23rd IEEE Convention of Electrical and Electronics Engineers in Israel, 2004.
6. J.K.S. Poon, J. Scheuer, Y. Xu, and A. Yariv, Designing coupled-resonator optical waveguide delay lines, J Opt Soc Am B 21 (2004), 1665–1673.
7. S. Mookherjea and A. Yariv, Second-harmonic generation with pulses in a coupled-resonator optical waveguide, Phys Rev E 65 (2002), 026607.
8. B.Z. Steinberg, Rotating photonic crystals: A medium for compact optical gyroscopes, Phys Rev E 71 (2005), 056621.
9. S. Boscolo, M. Midrio, and T.F. Krauss, Y junctions in photonic crystal channel waveguides: High transmission and impedance matching, Opt Lett 27 (2002), 1001–1003.
10. W.J. Kim and J.D. O'Brien, Optimization of a two-dimensional photonic crystal waveguide branch by simulated annealing and the finite-element method, J Opt Soc Am B 21 (2004), 289–295.
11. J. Smajic, C. Hafner, and D. Erni, Optimization of photonic crystal structures, J Opt Soc Am A 21 (2004), 2223–2232.
12. A. Mekis, J.C. Chen, I. Kurland, S. Fan, P.R. Villeneuve, and J.D. Joannopoulos, High transmission through sharp bends in photonic crystal waveguides. Phys Rev Lett 77 (1996), 3787–3790.
13. J.S. Jensen and O. Sigmund, Systematic design of photonic crystal structures using topology optimization: Low-loss waveguide bends. Appl Phys Lett 84 (2004), 2022–2024.
14. P.F. Xing, P.I. Borel, L.H. Frandsen, A. Harpøth, and M. Kristensen, Optimization of bandwidth in 60° photonic crystal waveguide bends, Opt Commun 248 (2005), 179–184.

15. M.P. Bendsøe and N. Kikuchi, Generating optimal topologies in structural design using a homogenization method, Comput Meth Appl Mech Eng 71 (1988), 197–224.
16. K. Svanberg, The method of moving asymptotes—A new method for structural optimization, Int J Numer Meth Eng 24 (1987), 359–373.
17. J.S. Jensen, O. Sigmund, L.H. Frandsen, P.I. Borel, A. Harpøth, and M. Kristensen, Topology design and fabrication of an efficient double 90° photonic crystal waveguide bend, IEEE Photon Technol Lett 17 (2005), 1202–1204.
18. P.I. Borel, A. Harpøth, L.H. Frandsen, and M. Kristensen, Topology optimization and fabrication of photonic crystal structures, Opt Express 12 (2004), 1996–2001.
19. J.S. Jensen and O. Sigmund, Topology optimization of photonic crystal structures: A high-bandwidth low-loss T-junction waveguide, J Opt Soc Am B 22 (2005), 1191–1198.
20. W.R. Frei, D.A. Tortorelli, and H.T. Johnson, Topology optimization of a photonic crystal waveguide termination to maximize directional emission. Appl Phys Lett 86 (2005), 111114.
21. J. Smajic, C. Hafner, and D. Erni, Design and optimization of an achromatic photonic crystal bend. Opt Express 11 (2003), 1378–1384.
22. T. Uusitupa, K. Kärkkäinen, and K. Nikoskinen, Studying 120° PBG waveguide bend using FDTD. Microwave Opt Technol Lett 39 (2003), 326–333.
23. R.E. Collin, Foundations for Microwave Engineering, McGraw-Hill, New York, 1992.
24. Y. Leviatan and A. Boag, Analysis of electromagnetic scattering from dielectric cylinder using a multifilament current model. IEEE Trans Antenn Propag 35 (1987), 1119–1127.

COMPACT SHARP CUTOFF WIDE STOPBAND LOW-PASS FILTER USING DEFECTED GROUND STRUCTURE AND SPURLINE

Santanu Dwari and Subrata Sanyal
Department of Electronics and Electrical Communication Engineering, Indian Institute of Technology, Kharagpur 721302, India

Received 3 March 2006

ABSTRACT: *A novel compact microstrip low-pass filter is proposed using defected ground structure and spurline. The measured passband to stopband attenuation slope is more than 73 dB/GHz. Electrical length of the filter is less than 20% of the guided wavelength at 3 dB cutoff frequency. Measured stopband attenuation is greater than 20 dB over more than 17.5 GHz band.* © 2006 Wiley Periodicals, Inc. Microwave Opt Technol Lett 48: 1871–1873, 2006; Published online in Wiley InterScience (www.interscience.wiley.com). DOI 10.1002/mop.21765

Key words: *low-pass filter; defected ground structure; spurline*

1. INTRODUCTION

PLANAR, compact low-pass filters (LPF) having sharp cutoff and wide stopband characteristics are of increasing demand in many RF and microwave applications such as rejection of harmonics and spurious signals. Conventional LPFs using shunt stubs and stepped impedance lines [1] have narrow stopband and poor cutoff response. LPFs using defected ground structures (DGS) were proposed in Refs. 2–6 to overcome the deficiencies of the conventional LPF. In Refs. 2 and 3, stopband attenuation are shown to be greater than 20 dB over a 6 GHz bandwidth while in Ref. 4, it is over about 5 GHz bandwidth. The LPF passband to stopband attenuation slope in Refs. 2–4 is less than 20 dB/GHz while that in Ref. 5 is better than 60 dB/GHz. However, in Ref. 5, the stopband attenuation remains below 18 dB over 2 GHz bandwidth and then rises to 5 dB over the next 2 GHz band. In Ref. 6, passband to stopband attenuation slope is better than 40 dB/GHz and the stopband attenuation is better than 18 dB over 6 GHz bandwidth.

In this paper, a new LPF is presented using DGS and spurline [7]. In the proposed filter, the DGSs are placed directly below spurline. In spurline, a $\lambda_g/4$ L-shaped thin slot is embedded in microstrip line, where λ_g is the guided wavelength of the microstrip line at the center frequency. The DGSs provide wide stop band. Spurline, without increasing size, gives attenuation poles at center frequency and at odd harmonics. This combination of DGS and spurline provides excellent LPF performance.

2. LPF USING DGS AND SPURLINE

Figure 1 shows the LPF using DGS, a spurline and proposed filter, which is a combination of DGS and spurline. In this paper, three square-head DGSs are used. The LPF is built on RT/Duriod 5880 (relative permitivity = 2.2 and thickness = 0.381 mm) substrate and simulations performed using a commercial full-wave electromagnetic simulator IE3D™. LPFs of proposed structure can be designed at different 3 dB cutoff frequencies by choosing suitable length of the LPF and size of the DGSs. To increase (decrease) the 3 dB cutoff frequency, the length of the LPF and size of the DGSs should be decreased (increased). Two examples of sharp cutoff wide stopband LPF of 3 dB cutoff frequency at 2.25 and 3.1 GHz are designed. For the first example, initially a LPF with DGSs and compensated microstrip line [4], as shown in Figure 1(a), is designed at 3 dB cutoff frequency at 2.85 GHz. Next, to get sharp cutoff, an L-shaped thin slot is embedded in compensated microstrip line. This however results in a slight shift of the 3 dB cutoff to 2.55 GHz. There is weak interaction between DGS and spurline.

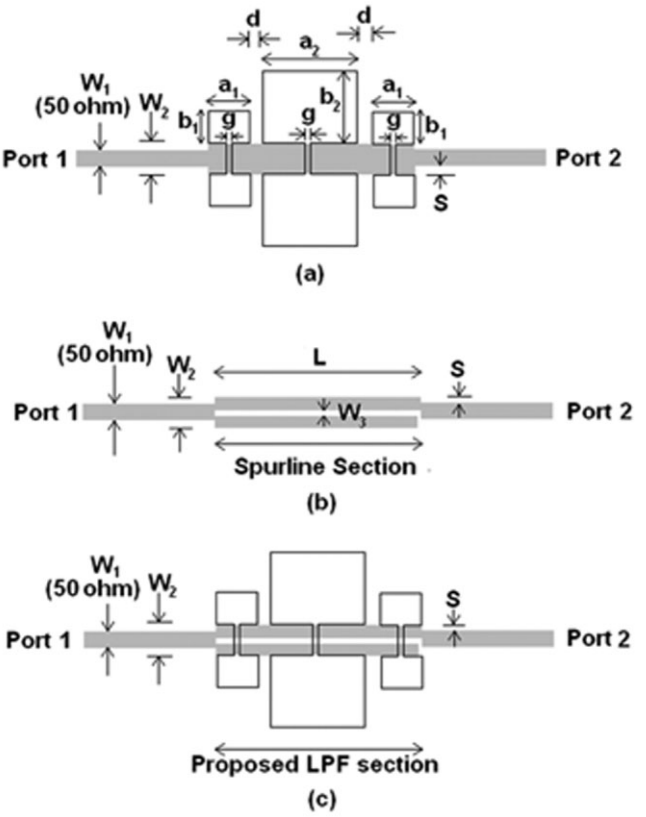

Figure 1 (a) LPF using DGS, (b) spurline section, (c) proposed LPF